# Supplementary information

## Influence of grain size on the solid-state direct reduction of polycrystalline iron oxide

Barak Ratzker[1,*], Martina Ruffino[1], Shiv Shankar[1], Yan Ma[1,2], Dierk Raabe[1,*]

[1] *Max Planck Institute for Sustainable Materials GmbH, Max-Planck-Str. 1, 40237 Düsseldorf, Germany*

[2] *Department of Materials Science and Engineering, Delft University of Technology, Mekelweg 2, 2628 CD Delft, the Netherlands*

* Corresponding authors: b.ratzker@mpi-susmat.de, d.raabe@mpi-susmat.de

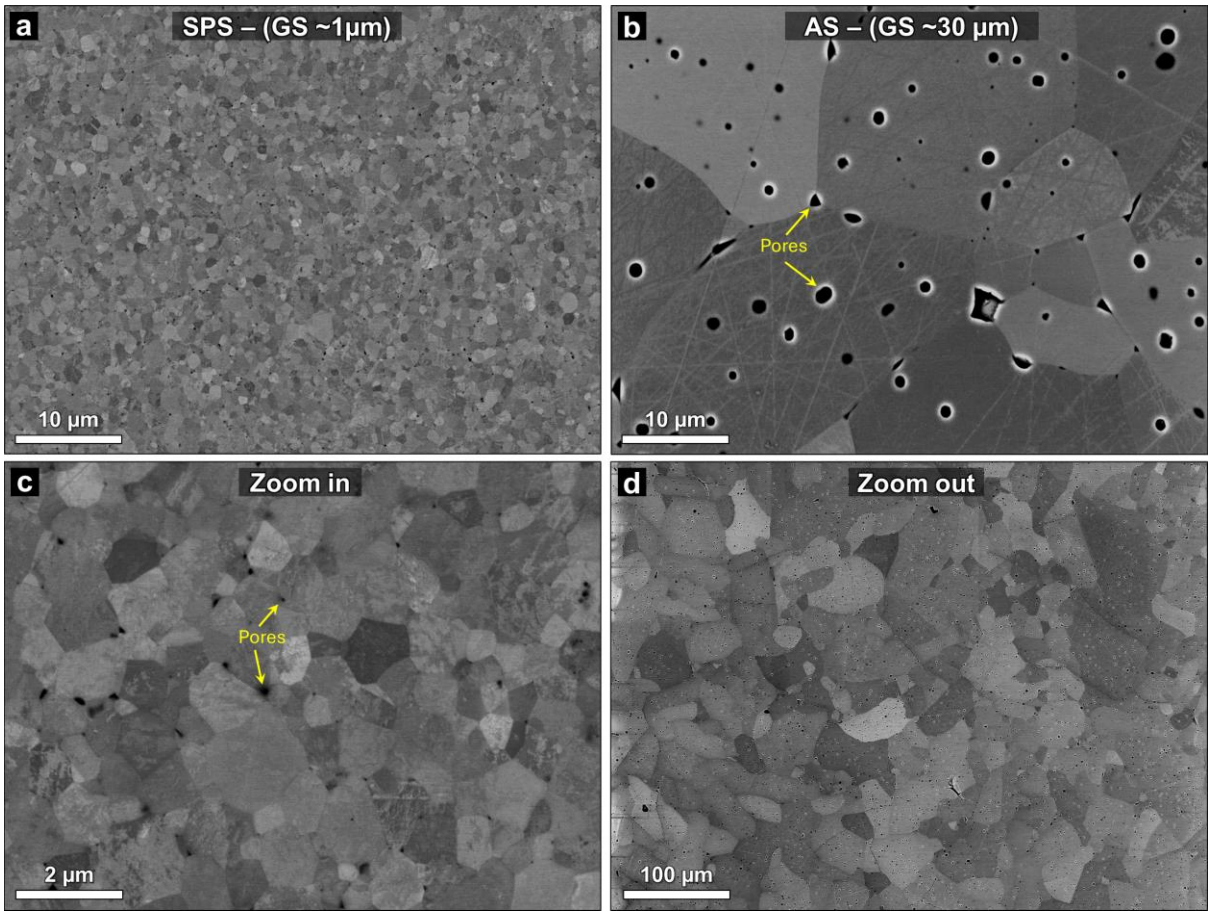


**Figure S1.** BSE-SEM images showcasing the microstructures of the (a) ultrafine and (b) large grain size hematite samples produced by spark plasma sintering (SPS) and air sintering (AS), respectively. (c) Higher magnification of the ultrafine grains and (d) low magnification of the large grains. Sintering pores can be observed in both materials; in the large-grained sample they are either intragranular and spherical (~1-2 μm in size) or at triple points, while in the ultrafine-grained sample they are all nanometric and only found at triple points.

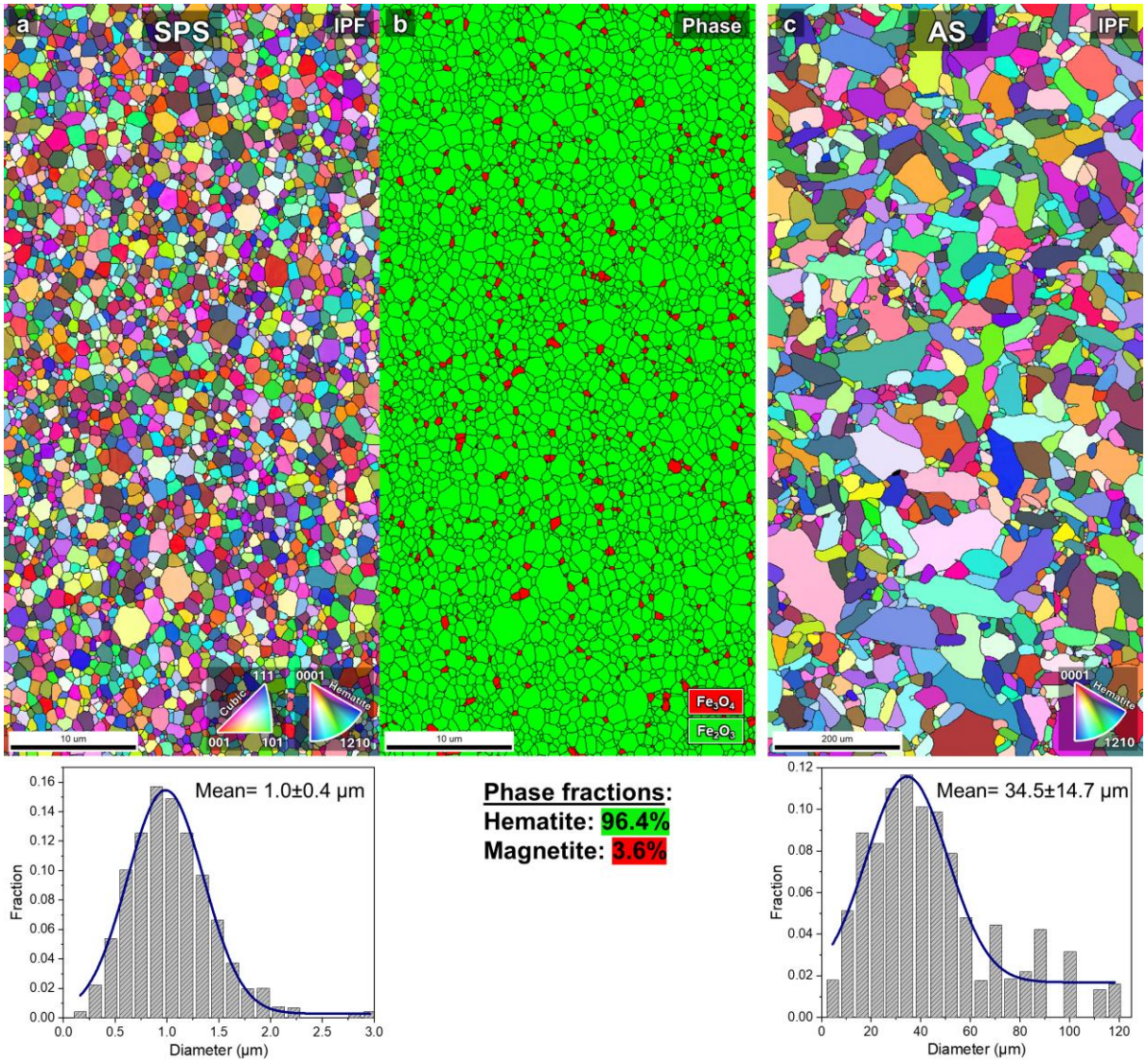


**Figure S2.** EBSD analysis of (a) SPSed ultrafine and (b) air sintered (AS) large grain size hematite, note that the scale bar in (b) is 20 times that in (a). In the SPSed ultrafine sample, as shown in the phase map, the original magnetite content (~3.5%) that was in the raw powder is retained due to the lack of oxidizing conditions during sintering. The corresponding grain size distributions for each material is respectively presented below the IPF.

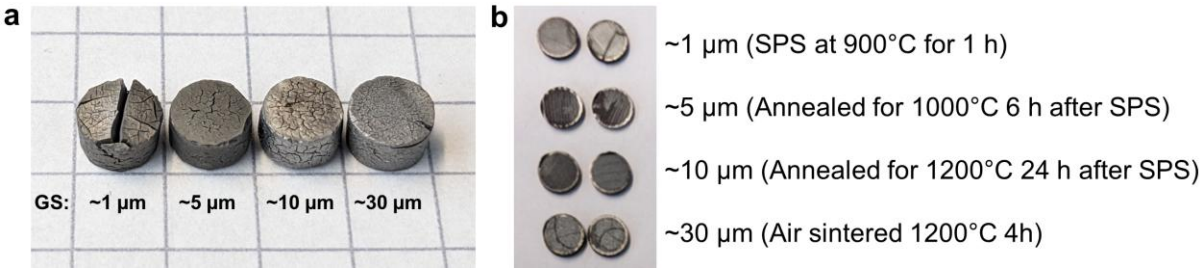


**Figure S3.** Photographs of samples with different grain sizes (a) after full reduction, 30 min at 700°C and (b) after partial reduction for 1 min at 700°C, cut in half across the circular cross-section.

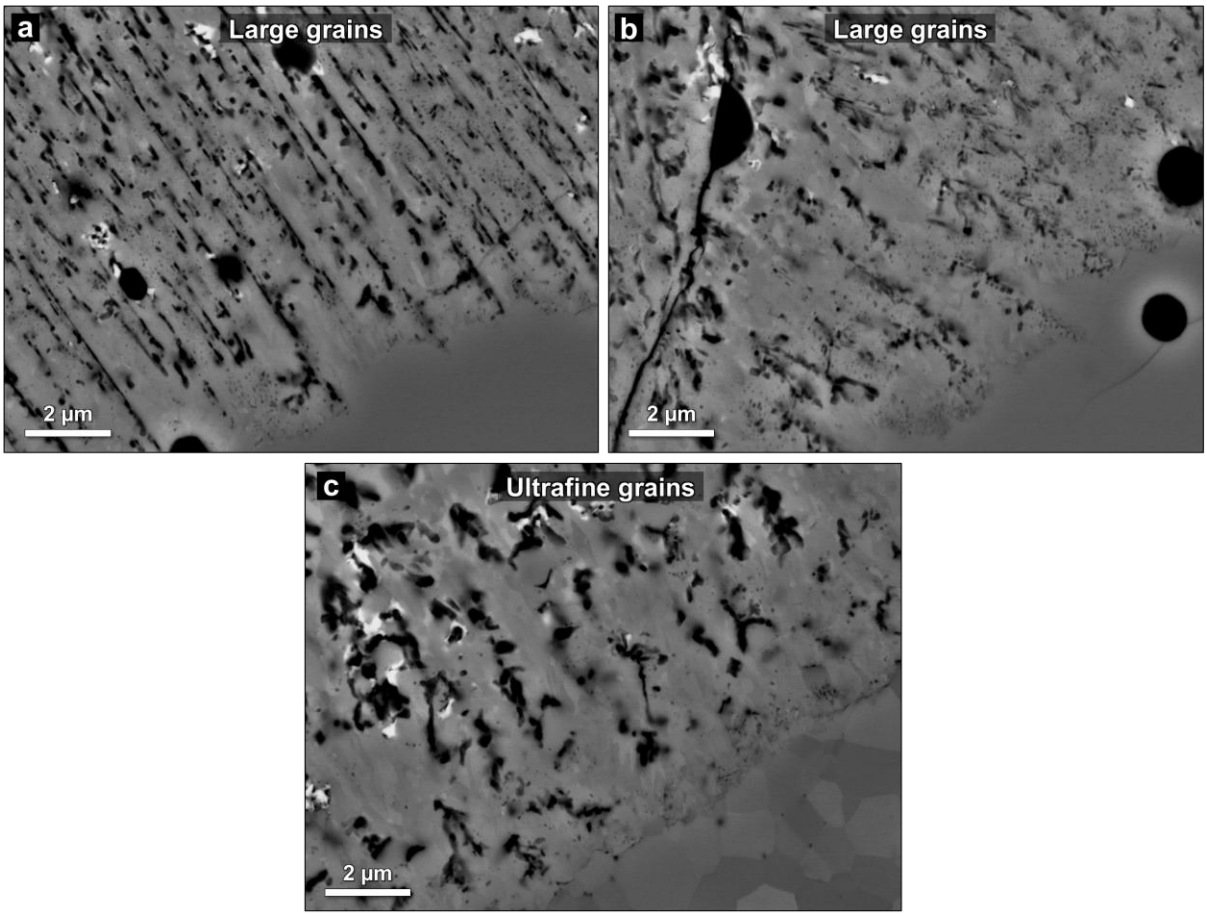


**Figure S4.** BSE-SEM high magnification images of the hematite/magnetite interface in (a) large grains with strong directionality of pore channels, (b) large grains with poor directionality, and (c) ultrafine grains with the characteristic inferior directionality. Note that the porosity created in the large grains is relatively fine regardless of directionality and that the porosity in the ultrafine-grained sample is comparatively coarse.

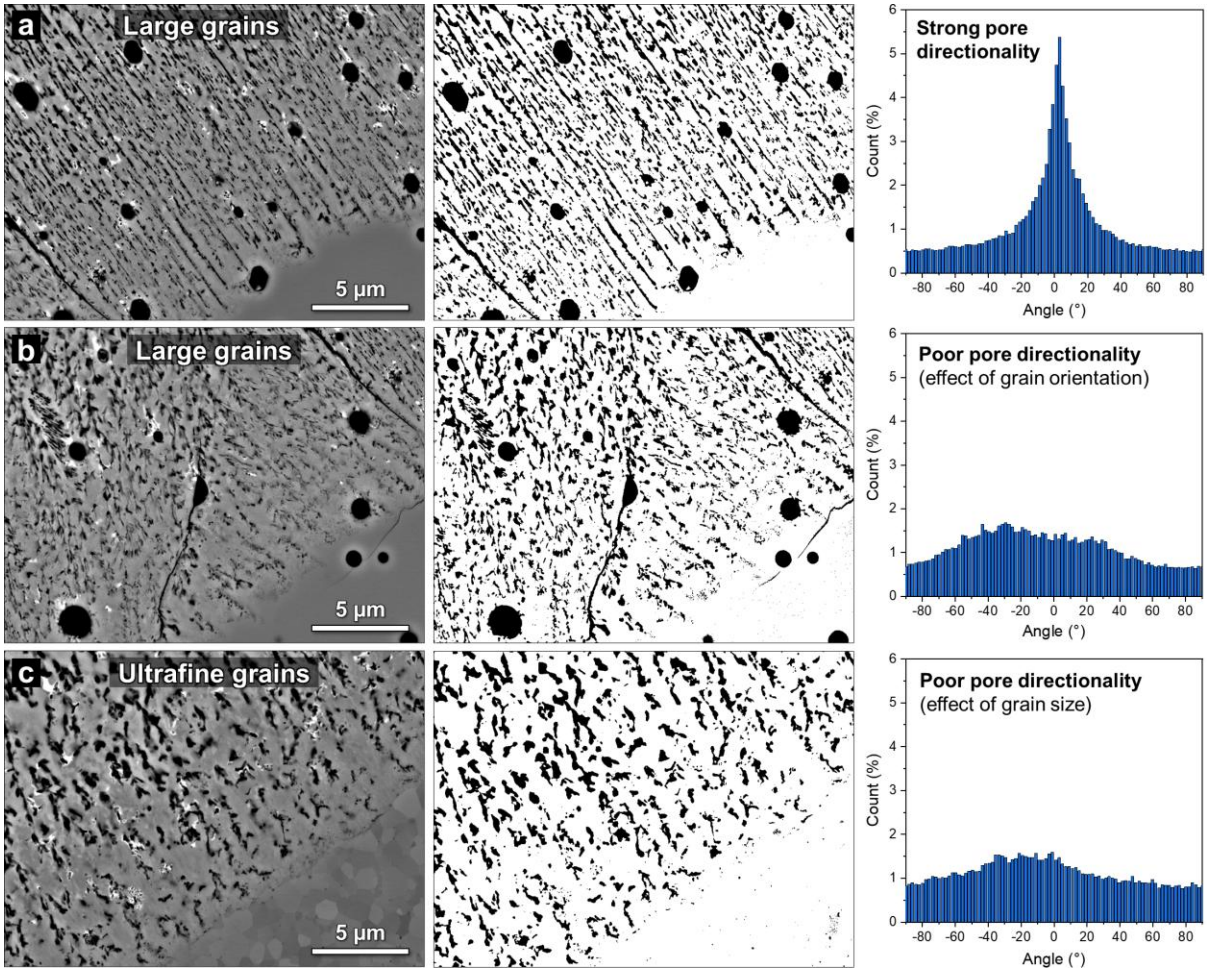


**Figure S5.** BSE-SEM images, image analysis of the porosity and the corresponding angular distribution of pores extended from the hematite/magnetite interface, illustrating the directionality in (a) large-grained region with strong pore directionality, (b) large-grained region with poor pore directionality, and (c) ultrafine-grained sample with poor pore directionality. Note that the deviation angle is calculated relative to the orientation of the interface.

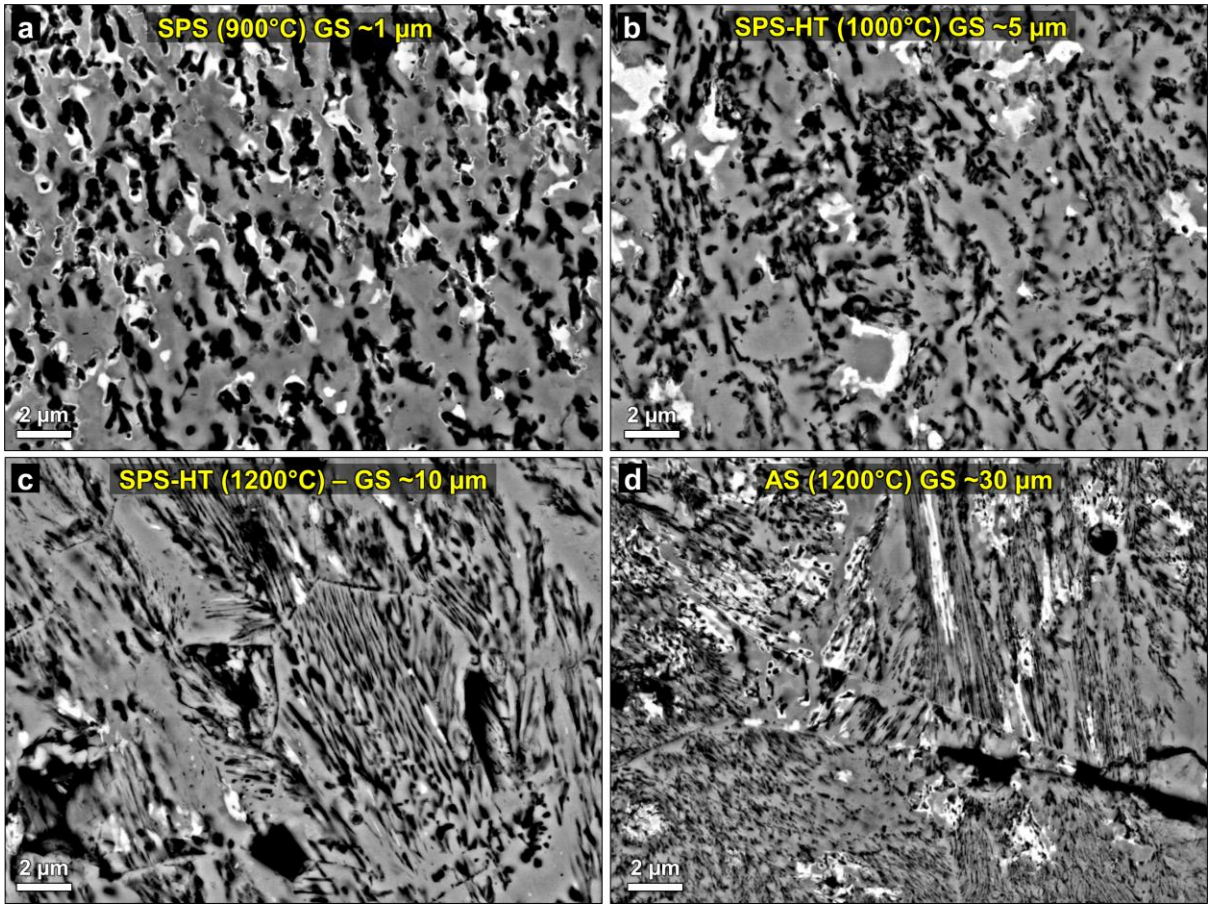


**Figure S6.** BSE-SEM cross section images taken at a distance roughly 30 µm away from the hematite interface, showcasing the porosity characteristics depending on grain size in partially reduced samples. (a) SPS at 900°C with ultrafine grains size of ~1 µm, (b) SPS + heat treatment at 1000°C for 6 h with grain size of ~5 µm, (c) SPS + heat treatment 1200°C for 24 h with grain size of ~10 µm, and (d) air sintered at 1200°C with a grain size of ~30 µm.

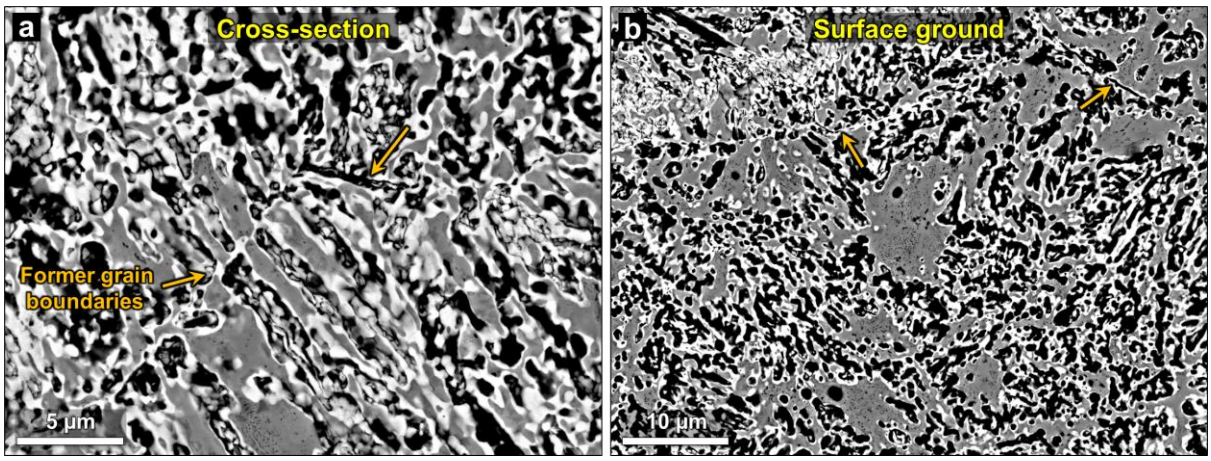


**Figure S7.** BSE-SEM images of Fe-rich regions in the reduced layer (a) cross section and (b) ground in surface, showing the typical larger trapped retained oxides that are found in the large-grained sample. Notice that many of these oxides still contain the initial very fine porosity that forms in the magnetite close to the hematite. Some of what used to be grain boundaries in the original hematite are marked with arrows.

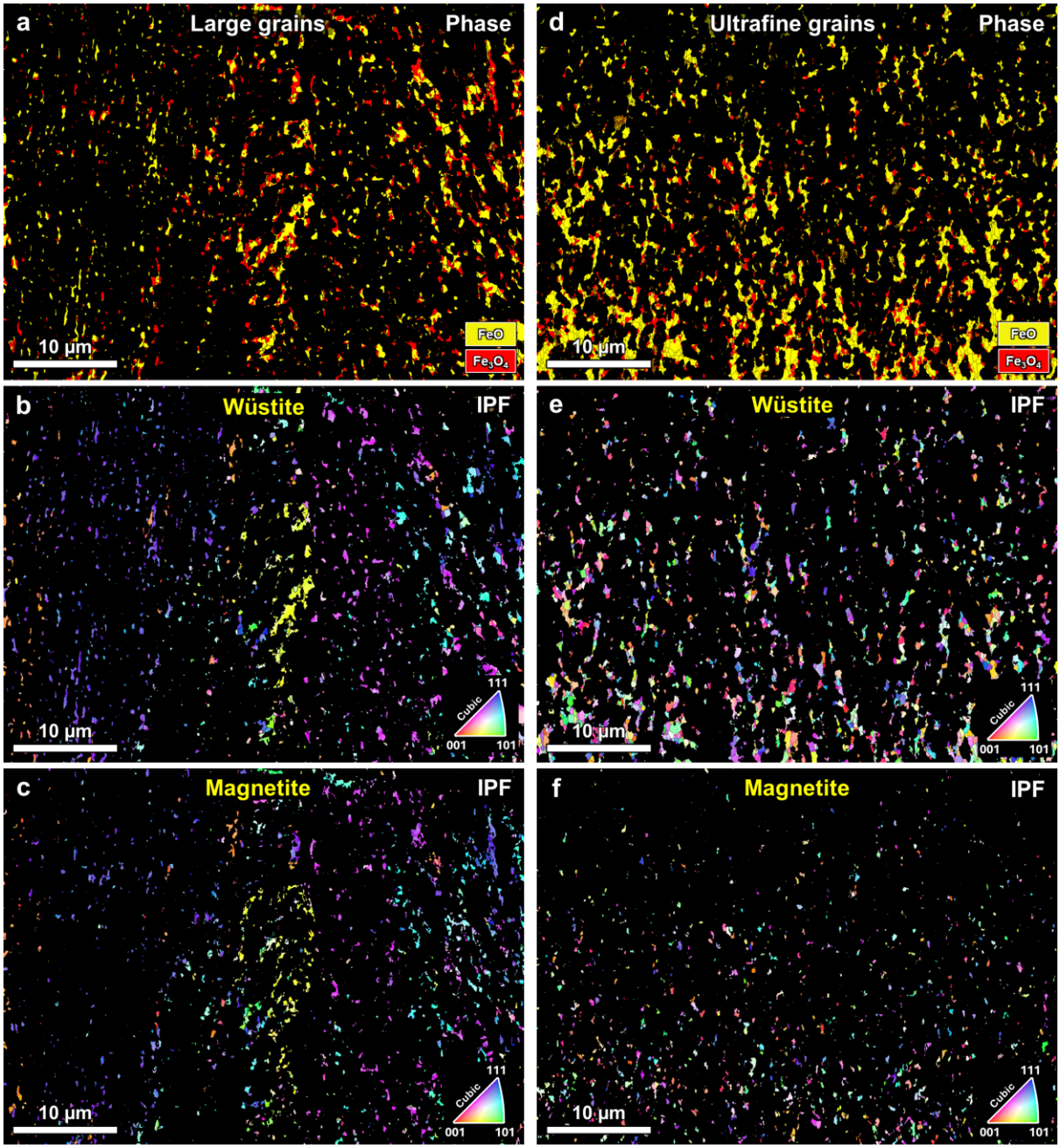


**Figure S8.** EBSD analysis of oxides phases in iron-rich regions of the reduced layers. Large-grained sample: (a) phase map, and IPF partitioning of (b) wüstite and (c) magnetite. Ultrafine-grained sample: (d) phase map, and IPF partitioning of (e) wüstite and (f) magnetite. There is evident local texture in the wüstite and magnetite along the reduction direction only in the reduced large hematite grain size sample.

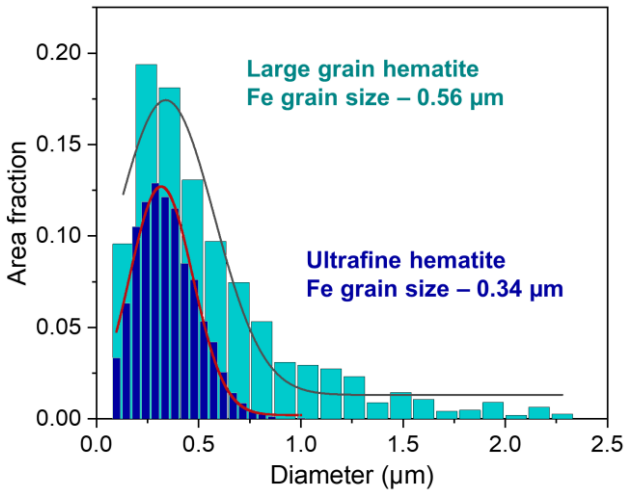


**Figure S9.** Grain size distribution of the Fe grains in the reduced regions of the partially reduced samples that initially had an ultrafine (blue) and large (cyan) hematite grain size.

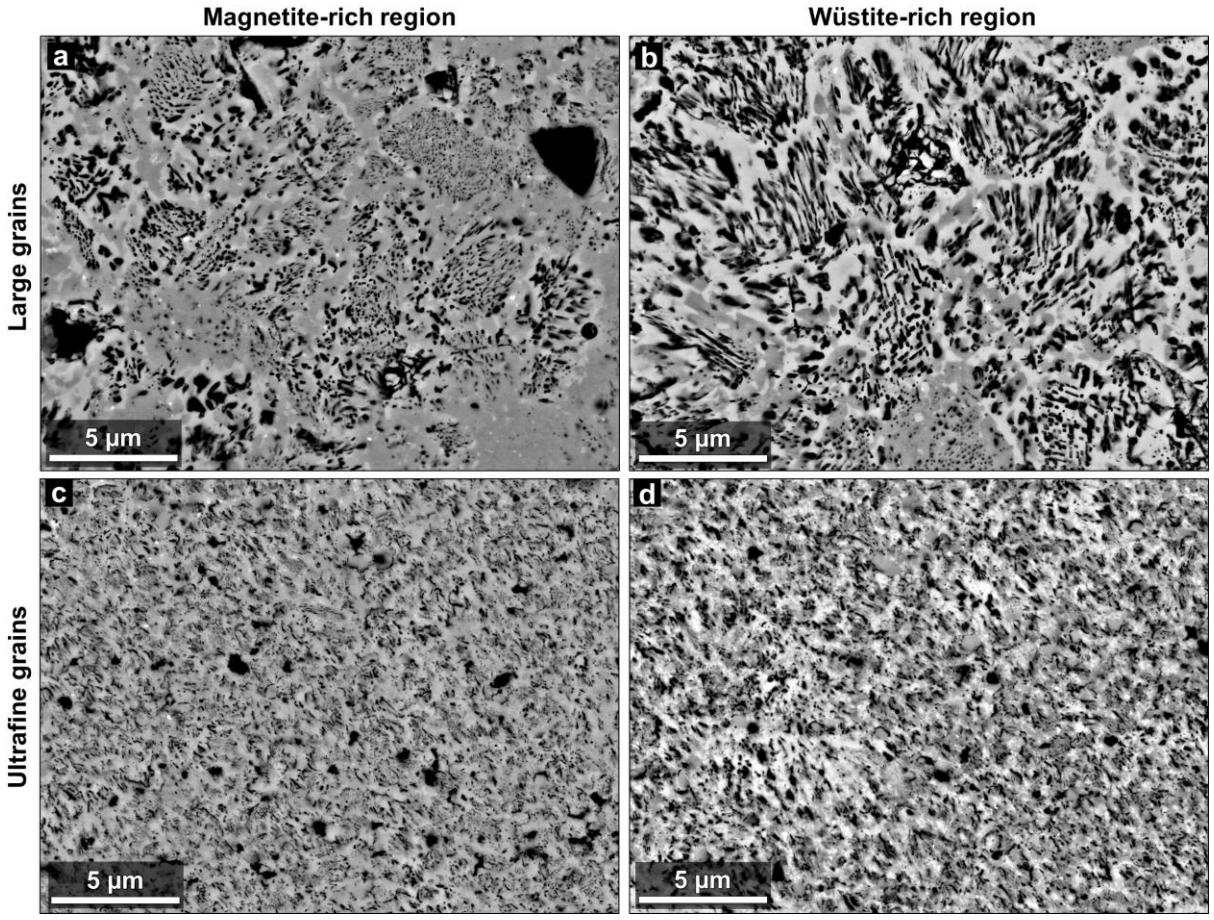


**Figure S10.** Microstructure of partially reduced samples as seen by grinding into the interface showing the developed "cell structure" in the oxide-rich regions. Large grains sample at (a) magnetite- and (b) wüstite-rich regions. Ultrafine grains sample at (c) magnetite- and (d) wüstite-rich regions. The darker and lighter grey oxides phases correspond to magnetite and wüstite, respectively.

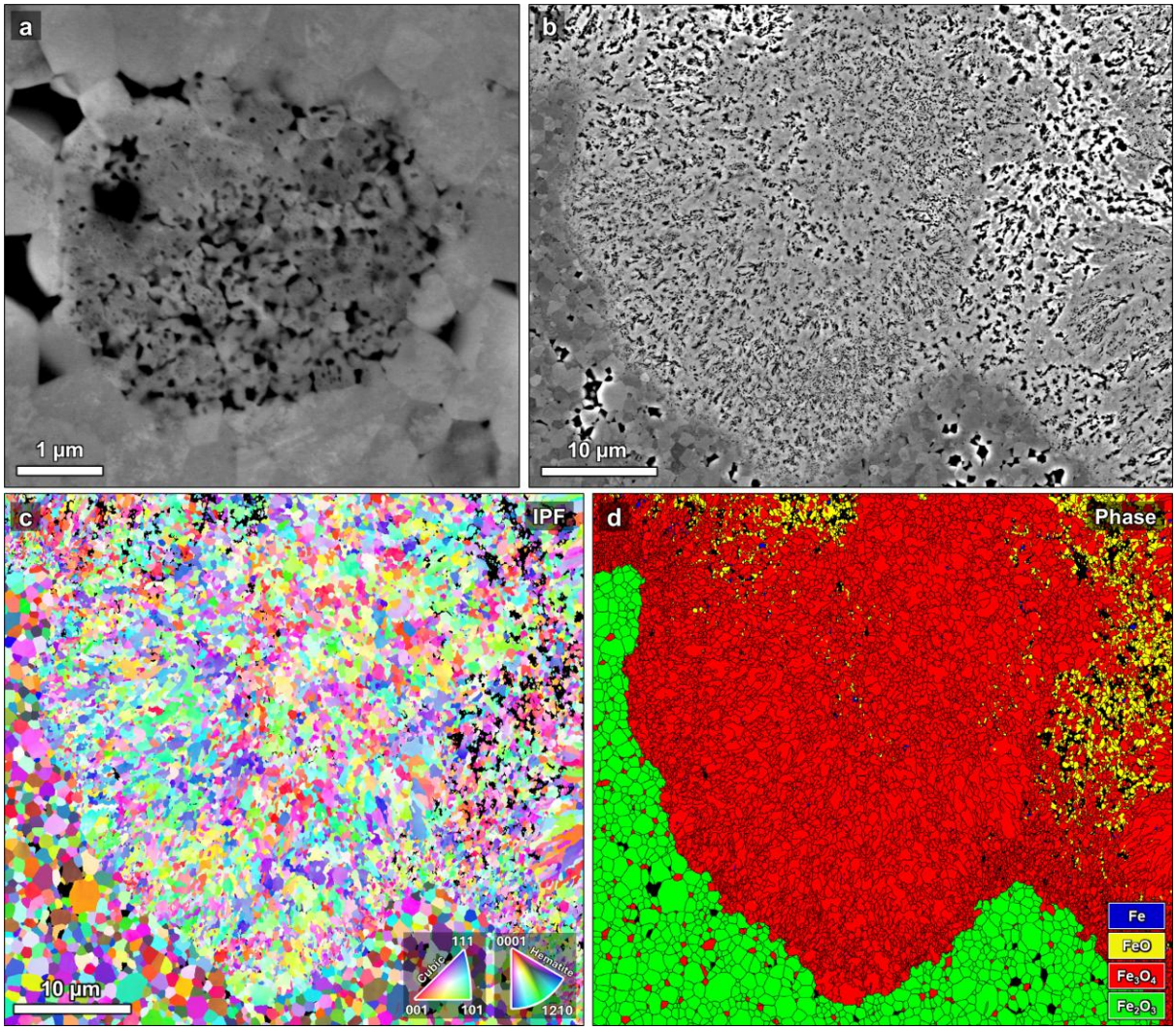


**Figure S11.** Microstructure of the partially reduced ultrafine-grained hematite ground in from the reduced surface. (a) High and (b) low magnification BSE-SEM images showing the lack of a "cell structure" in the magnetite at the hematite interface. EBSD analysis (c) IPF and (d) phase map revealing the magnetite structure near the hematite interface.

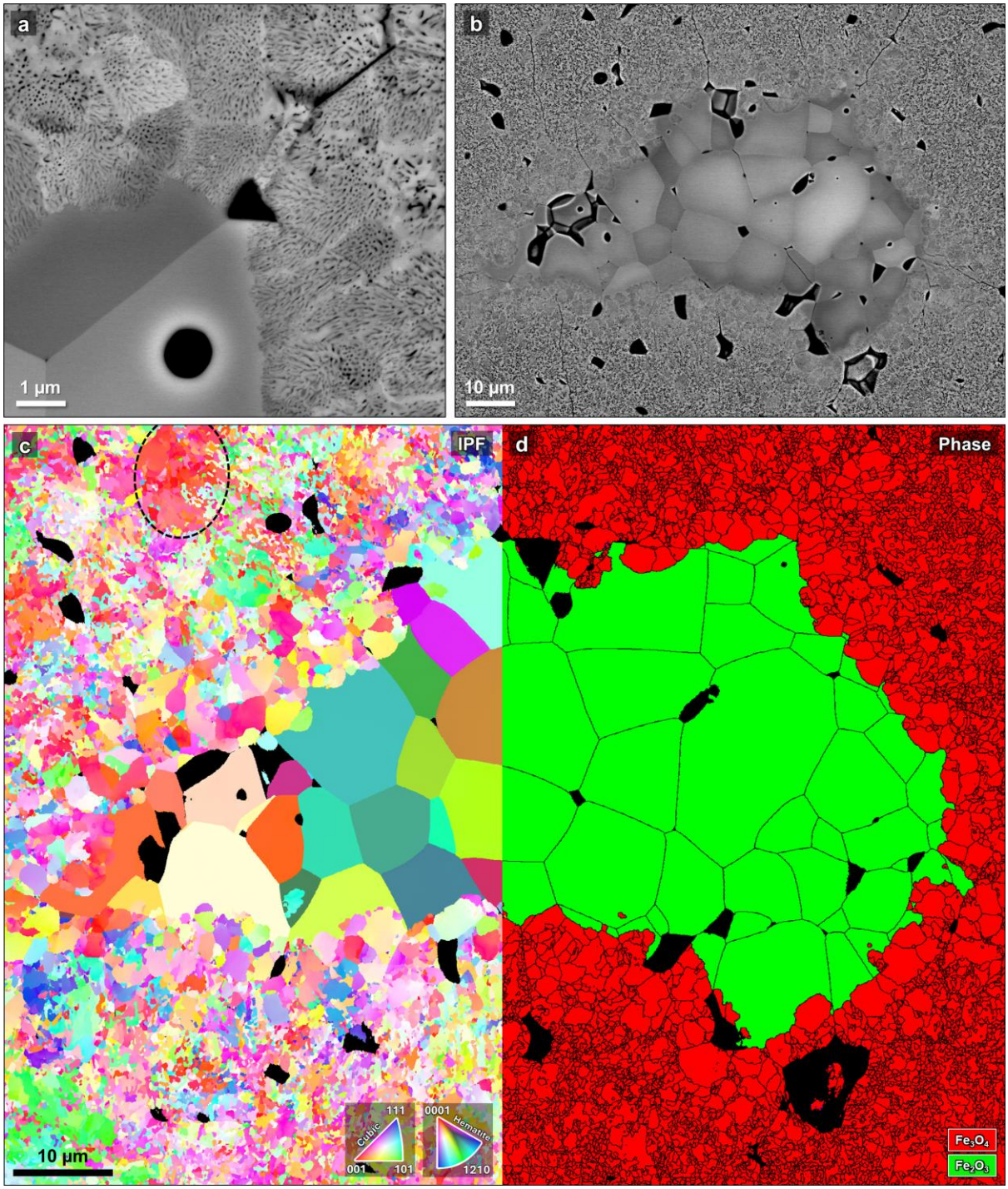


**Figure S12.** Microstructure of the partially reduced large-grained hematite ground in from the reduced surface. (a) High and (b) low magnification BSE-SEM images showing the distinct "cell structure" in the magnetite at the hematite interface. EBSD analysis (c) IPF and (d) phase map revealing the magnetite structure near the hematite interface. Local texturing related to the precursor large hematite grains can be observed, see for example the red region circled with the dashed line in (c). Significant grain refinement is observed following the initially large "cell structure" magnetite grains.